AFRL-RX-WP-TP-2011-4087

ELECTRICAL CONDUCTIVITY MANIPULATION AND SWITCHING PHENOMENA OF POLY(p-PHENYLENEBENZOBISTHIAZOLE) THIN FILM BY DOPING PROCESS (PREPRINT)

Jiahua Zhu, Thomas C. Ho, Zhanhu Guo, and Suying Wei

Lamar University

Sung Park

Northrop Grumman Corporation

Max Alexander

Composite and Hybrid Materials Branch
Nonmetallic Materials Division

OCTOBER 2010

AIR FORCE RESEARCH LABORATORY
MATERIALS AND MANUFACTURING DIRECTORATE
WRIGHT-PATTERSON AIR FORCE BASE, OH 45433-7750
AIR FORCE MATERIEL COMMAND
UNITED STATES AIR FORCE

REPORT DOCUMENTATION PAGE

Form Approved
OMB No. 0704-0188

1. REPORT DATE *(DD-MM-YY)*	2. REPORT TYPE	3. DATES COVERED *(From - To)*
October 2010	Technical Paper Preprint	21 October 2008 – 21 October 2010

4. TITLE AND SUBTITLE

ELECTRICAL CONDUCTIVITY MANIPULATION AND SWITCHING PHENOMENA OF POLY(p-PHENYLENEBENZOBISTHIAZOLE) THIN FILM BY DOPING PROCESS (PREPRINT)

5a. CONTRACT NUMBER
In-house

5b. GRANT NUMBER

5c. PROGRAM ELEMENT NUMBER
62102F

6. AUTHOR(S)

Jiahua Zhu, Thomas C. Ho, Zhanhu Guo, and Suying Wei (Lamar University)
Sung Park (Northrop Grumman Corporation)
Max Alexander (AFRL/RXBC)

5d. PROJECT NUMBER
4347

5e. TASK NUMBER
33

5f. WORK UNIT NUMBER
BN103200

7. PERFORMING ORGANIZATION NAME(S) AND ADDRESS(ES)

Lamar University
Beaumont, TX 77710

Northrop Grumman Corporation
One Hornet Way, MIS: 9A45 W2
El Segundo, CA 90245

Composite and Hybrid Materials Branch (AFRL/RXBC)
Nonmetallic Materials Division, Air Force Research Laboratory
Materials and Manufacturing Directorate
Wright-Patterson Air Force Base, OH 45433-7750
Air Force Materiel Command, United States Air Force

8. PERFORMING ORGANIZATION REPORT NUMBER
AFRL-RX-WP-TP-2011-4087

9. SPONSORING/MONITORING AGENCY NAME(S) AND ADDRESS(ES)

Air Force Research Laboratory
Materials and Manufacturing Directorate
Wright-Patterson Air Force Base, OH 45433-7750
Air Force Materiel Command
United States Air Force

10. SPONSORING/MONITORING AGENCY ACRONYM(S)
AFRL/RXBC

11. SPONSORING/MONITORING AGENCY REPORT NUMBER(S)
AFRL-RX-WP-TP-2011-4087

12. DISTRIBUTION/AVAILABILITY STATEMENT
Approved for public release; distribution unlimited.

13. SUPPLEMENTARY NOTES
PAO Case Number: 88ABW-2010-5914; Clearance Date: 05 Nov 2010. Report contains color.

14. ABSTRACT

Current-voltage (i-v) characteristics of dry poly(p-phenylenebenzobisthiazole) (PBZT) thin films are studied before and after various doping processes, Conductivity switching phenomenon is observed after doping with HCI and H_2SO_4 acidic solutions at different concentration levels. The conductivity is 10 folds higher in a relatively high sweeping voltage range (0.2-0.3 V) than that sweeping in lower range of 0-0.1V. Conductivity switching phenomenon becomes more obvious with an increase of acid concentration. HCI shows more favorable for a quick and efficient behavior than H_2S0_4, Reduction of PBZT with metal (Fe, Cu, and Pd) doping process produces a linear conductivity along the whole sweeping range of voltage. A 30% electrical conductivity enhancement is observed after applying an external dc voltage on the acid soaked PBZT film and different voltages enhance the conductivity to the same level. The conductivity returns gradually after removing the applied voltage. Four-probe conductivity measurements, FT-IR, scanning electron microscopy, EDAX elemental analysis, x-ray diffraction and TGA thermal analysis were used for better understanding the doping processes and conductivity switching mechanisms. A molecular structure transformation during the doping process is proposed.

15. SUBJECT TERMS
conductivity, PBZT, thin films

16. SECURITY CLASSIFICATION OF:			17. LIMITATION OF ABSTRACT:	18. NUMBER OF PAGES	19a. NAME OF RESPONSIBLE PERSON (Monitor)
a. REPORT	b. ABSTRACT	c. THIS PAGE			Max Alexander
Unclassified	Unclassified	Unclassified	SAR	26	19b. TELEPHONE NUMBER *(Include Area Code)* N/A

Electrical Conductivity Manipulation and Switching Phenomena of Poly(p-phenylenebenzobisthiazole) Thin Film by Doping Process

Jiahua Zhu[1], Suying Wei[2], Sung Park[3], John Willis[3], Max Jr. Alexander[4], Thomas C. Ho[1], and Zhanhu Guo[1*]

[1]Integrated Composites Laboratory (ICL)
Dan F Smith Department of Chemical Engineering
Lamar University, Beaumont, TX 77710, USA

[2] Department of Chemistry and Physics, Lamar University, Beaumotn, TX 77710, USA

[3]Advanced Materials and Process Development, NGC ISWR, One Hornet Way, M/S: 9A45 W2 El Segundo, CA 90245, USA

[4]Electromagnetic Hardened Materials, Materials and Manufacturing Directorate, Air Force Research Laboratory, Wright-Patterson, AFB, OH 45433-7750, USA

* Corresponding author: zhanhu.guo@lamar.edu; Phone: (409) 880-7654

Current-voltage (i-v) characteristics of dry poly(p-phenylenebenzobisthiazole) (PBZT) thin films are studied before and after various doping processes. Conductivity switching phenomenon is observed after doping with HCl and H_2SO_4 acidic solutions at different concentration levels. The conductivity is 10 folds higher in a relatively high sweeping voltage range (0.2-0.3 V) than that sweeping in a lower range of 0-0.1 V. Conductivity switching phenomenon becomes more obvious with an increase of acid concentration. HCl shows more favorable for a quick and efficient switching behavior than H_2SO_4. Reduction of PBZT with metal (Fe, Cu and Pd) doping process produces a linear conductivity along the whole sweeping range of voltage. A 30% electrical conductivity enhancement is observed after applying an external dc voltage on the acid soaked PBZT film and different voltages enhance the conductivity to the same level. The conductivity returns gradually after removing the applied voltage. Four-probe conductivity measurements, FT-IR , scanning electron microscopy, EDAX elemental analysis, X-ray diffraction and TGA thermal analysis were used for better understanding the doping processes and conductivity switching mechanisms. A molecular structure transformation during the doping process is proposed.

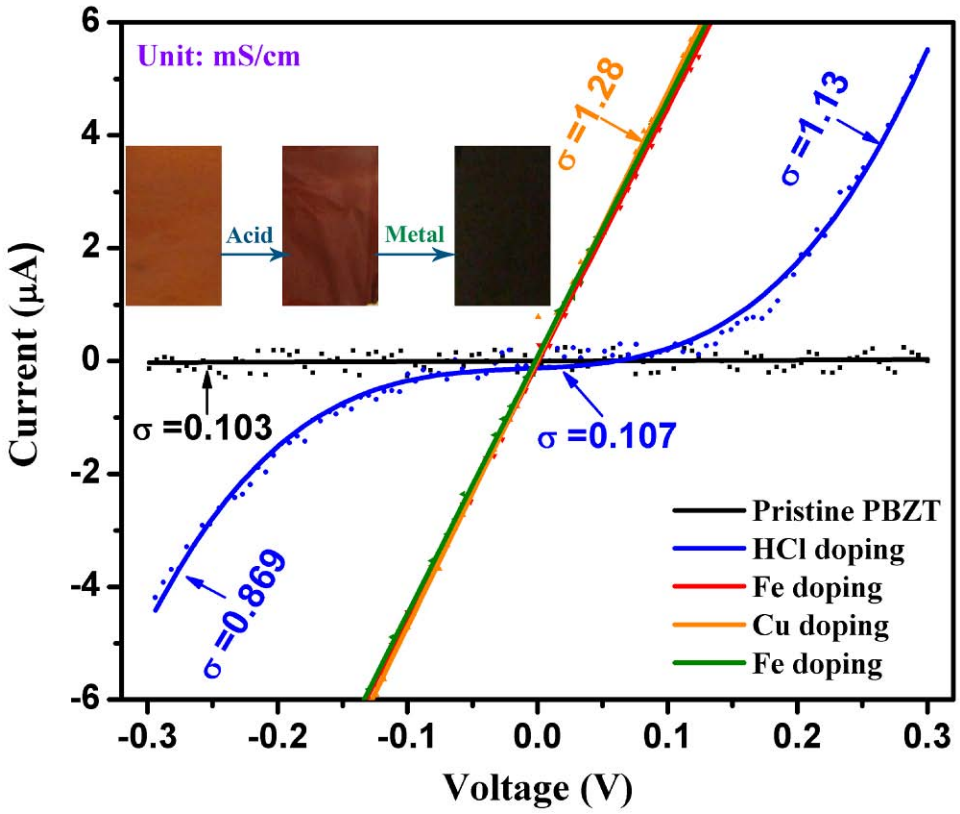

1. Introduction

Conductive polymers have attracted considerable attention due to their unique and tunable electronic, optical, physical, chemical, and electro-chemical properties.[1-4] The conductive polymers with facile interconversion of redox states could have different conductive attributes varying from metallic, semi-conductive to insulating, which strongly depends on the doping. Different doping methods such as Solvato-Controlled doping,[5] self-acid doping[6] and corolla discharge,[7] have been introduced to change the redox states in the conductive polymers. The doped conductive polymers have unique properties including polymer conformation, doping level, conductivity and color, which make them good potential candidates for applications such as displays, energy storage devices, actuators, and sensors.[2-4, 8-16]

Poly(p-phenylenebenzobisthiazole) (PBZT) has strong mechanical properties (tensile moduli of 240 and 300 GPa and strengths of 1.5 and 3 GPa), impressive thermal stability (retaining its mechanical properties to 650 ^{o}C) and good resistance to solvents and acids.[17-20] PBZT has potential applications in electronics,[21] light emitting diodes(LEDs),[22] and fuel cells.[23] However, there are two major challenges for the potential application of PBZT. One is the relatively lower axial compressive strength as compared to that of the carbon and inorganic fibers.[24] Several attempts have been made to improve the compressive strength of these highly oriented materials, including the polymer infiltration[25] and polymer structure change by introducing strong association groups,[26] branching[27] and cross-linking.[28, 29] The other is the poor solubility. Michael et al[30] found that PBZT can only dissolve in strong acids such as methanesolfonic acid (MSA) and chlorosulfonic acid (CSA), which is due to the rigid-rod like conformation with a very high packing of the chains, and strong intramolecular and intermolecular forces. Jenekhe[31,32] reported that PBZT and other rigid-chain polymers can be solubilized in aprotic organic solvents in the presence of metal halide Lewis acids such as $AlCl_3$, $FeCl_3$, and $GaCl_3$. All these progress for the above challenges provide a great opportunity to explore the potential applications of PBZT for devices with flexible morphology control, required miniaturization and more efficiency.

Recently, switchable electrical conductivity was reported in the nanomaterials functionalized with conjugated polymers. Wang et al[33] found that p-n junction is formed when ZnO nanowires are functionalized with p-type oligomer. This material served as a “diodes” that control the flow of current. Wang et al[34] applied mechanical stress to change the pathways of electrons of Au nanoparticle/citrate self-assembling film and thus the molecular conductivity. However, there is no switching phenomenon reported on PBZT film, especially under dry

conditions. PBZT exhibits quite interesting and unusual optical and electrical properties, highly depending on the presence of an acid within the film with an ability to protonate the nitrogen sites in the aromatic heterocycle.[35]

In this work, switching electrical conductivity of PBZT film is firstly reported after doping with HCl and H_2SO_4 at different pH levels. The electrical conductivity is enhanced significantly with an increase of sweeping voltage. Doping the protonated PBZT with metal improves the electrical conductivity tremendously and the switching phenomenon is disappeared. Applying external voltage shows further enhancement of conductivity. The switching mechanism is proposed in this work.

2. Experimental

2.1 Materials

PBZT thin films (6~8 μm) were provided by the Air Force research laboratory. HCl (37 wt%) and H_2SO_4 (95-98 wt%) were purchased from Sigma Aldrich. Copper (Cu), iron (Fe) and palladium (Pd) wires were commercially purchased. All the materials were used as received without further treatment.

2.2 Preparation of Doped PBZT Samples

2.2.1. PBZT Protonation Different concentrations of both aqueous HCl and H_2SO_4 were prepared: HCl (14.3 wt%, 24.2 wt%, 31.4 wt%, 37 wt%), H_2SO_4 (15 wt%, 35 wt%, 47 wt%, 55 wt%). PBZT was immersed in DI water prior to use. For acid doped samples, PBZT was immersed in different acid solutions for 5 min (color changed from yellow to orange) and then

moved out, sopped up the residue solution on the PBZT surface and then left the samples at ambient condition for another 15 min.

2.2.2 Metal Doping The PZBT thin film doped with metal was carried out according to the following procedures. PBZT thin film was firstly protonated by strong acid. Both 37 wt% HCl and 55 wt% H_2SO_4 were tested. The protonated PBZT thin film was touched by a thin metal wire, as seen in Figure 1. The color of the contact area turned to black immediately and expanded to the entire PBZT surface.

2.3 Characterization

The morphology of the pristine PBZT and doped PBZT was evaluated using scanning electron microscopy (Hitachi S-3400 scanning electron microscopy). The EDAX attached to scanning electron microscope was used to characterize the elemental component for both pristine PBZT and PBZT thin films doped with acids and metals. Fourier transform infrared spectroscopy (FT-IR, a Bruker Inc. Tensor 27 FT-IR spectrometer with hyperion 1000 ATR microscopy accessory) was used to characterize the pristine PBZT and doped PBZT thin films.

The crystal structure of the pristine PBZT, acid-doped and metal-doped PBZT thin film was investigated by powder X-ray diffraction. The powder X-ray diffraction analysis of the samples was carried out with a Bruker AXS D8 Discover diffractometer with GADDS (General Area Detector Diffraction System) operating with a Cu-Ka radiation source filtered with a graphite monochromator (λ=1.5406Å). The detector used was a HI-STAR two-dimensional multi-wire area detector. The samples were loaded onto double sided scotch tape, placed on a glass slide, and mounted on a quarter-circle Eulerian cradle (Huber) on an XYZ stage. The X-ray beam was generated at 40 kV and 40 mA power and was collimated to about an 800-mm spot

size on the sample. The incident ω angle was 5°. A laser/video system was used to ensure the alignment of the sample position on the instrument center. XRD scans were recorded from 5 to 40° for 2θ with a 0.050° step-width and a 60-s counting time for each step. The XRD data were analyzed using the DIFFRAC-Plus EVA program (Bruker AXS, Karlsruhe, Germany), and the patterns were identified using the ICDD PDFMaint computer reference database.

The electrical conductivity of each sample was measured by a four-probe technique (C4S 4-Point Probe Head, Cascade Microtech. Tips are made of tungsten carbide.), Figure 2(a). To make sure that a precise voltage is applied on the two inner probes, V-source testing mode (Keithley 2400 source meter, USA) is introduced. The measured voltage is adjusted in the range of -0.3 V to 0.3 V and the corresponding current is measured and recorded across the two outer probes. Dimensions of the film used are 10 mm×5 mm×0.08 mm.

External voltages (bias) are applied (3 V, 5 V and 10 V) on PBZT surface by a DC power unit (TEKPOWER HY1803D). To avoid natural doping of copper wire, carbon fiber (CF) matrix is used as electrode and the distance between the two carbon fiber electrodes is adjusted about 40 mm. During measurement, a thin layer of 55 wt% H_2SO_4 is covered on the PBZT surface to promote the conductivity, Figure 2(b). Four-point measurement is conducted both when the external voltage is on and off.

Electrical resistivity (ρ, Ω·cm) of the thin film is calculated according to Equqtion (1).[36, 37]

$$\rho = \frac{V \times 2\pi}{I \times (\frac{1}{S_1} + \frac{1}{S_2} - \frac{1}{S_1 + S_2} - \frac{1}{S_2 + S_3}) \times CF} \quad (1)$$

where, V (V) is the potential difference between the two inner probes, I (A) is the electrical current that flows through the outer pairs of probes, S_n (mm) represents the distances between the two adjacent probes and CF is the correction factor that depends on W (mm) and S_n. In this case,

the resistivity is measured after placing the test piece on a non-conducting surface. This corresponds to the seventh case reported by Valdes,[36] for which the correction coefficient factor is shown in Equation (2).

$$CF = 1 + 4\frac{S}{W}\sum_{n=1}^{\infty}\left(\frac{1}{\sqrt{\left(\frac{S}{W}\right)^2 + 4n^2}} - \frac{1}{\sqrt{\left(\frac{2S}{W}\right)^2 + 4n^2}}\right) \quad (2)$$

where, S is the average distance among the probes, and W is the thickness of the test piece. Thus, the electrical conductivity (σ,S/cm) is obtained by Equation (3).

$$\sigma = \frac{1}{\rho} \quad (3)$$

3. Results and discussion

3.1 Electrical Conductivity Switching Phenomenon

3.1.1 Without An Applied External Voltage

Figure 3 shows the electrical conduction variation of the dry PBZT films doped with both HCl and H_2SO_4 acid of different concentrations. The electrical conductivity of the pristine PBZT is calculated to be 1.03×10^{-4} S/cm without any doping and remains constant during the sweeping range of -0.3 V ~ 0.3 V. The non-linear electrical conductivity (switching phenomenon) is observed and varies with the sweeping voltages after PBZT is doped with acid. The conductivity of the PBZT doped with 24.2 wt% HCl is about 7-10 times larger than that of the pristine PBZT. However, the switching behavior is not so obvious in the PBZT doped with H_2SO_4 as compared to that in the HCl doped ones. A 5-8 times enlarged conductivity is observed in the voltage range of 0.2 V ~ 0.3 V as compared to that at lower voltage, Figure 3(a) and (c). In addition, the conductivity switches to much higher value at relatively higher voltage (-0.2 V ~ -0.3 V; 0.2 V ~ 0.3 V). The non-linear conductivity is also reported on poly(benzimidazobenzophenanthroline)[38]

and polypeptide membrane[39] in the electrolyte solution, but the conductivity strongly depends on the pH value and the electrolyte used in the solution. In this work, acid is used as a dopant to protonate PBZT and removed before the test. More obvious switching phenomenon is observed in the PBZT thin film doped with higher concentrated acid, Figure 3(b) and (d).

However, the switching behavior of conductivity disappears again after doping with metals (Fe, Cu and Pd). Same conductivity is obtained after doping with different metals. This represents a characteristic distinctive of a localized-state, electron-hopping, redox conductor, where the occupied and unoccupied electron sites within the film have become completely concentration polarized. Similar results are reported on dried poly(benzimidazobenphen anthroline).[38] Meanwhile, the conductivity is not strongly depending on the acid after doping metals, the similar conductivity is observed for HCl (1.28 S/cm) and H_2SO_4 (1.36 S/cm) protonated samples. Comparing with that of the pristine PBZT, the conductivity of metal doped PBZT increases by 12 times and keeps constant during the sweeping range.

3.1.2 With An Applied External Voltage

Figure 5(a) shows the effect of applied external voltage on the electrical conductivity (σ) of 55 wt% H_2SO_4 doped PBZT samples. A relative large dc potential bias produces dc redox construction currents that reach voltage-independent plateau when the polymer's electron occupancy sites become completely polarized.[38] The conductivity reaches the similar high plateau after applying different levels of voltage (3V, 5V and 10V), which increases significantly fast, about 30% within seconds. The conductivity is constantly stable at the high plateau within the initial 10 min while applying the voltage. This is due to the localized electrons on the identifiable molecular sites in the polymer, which are transported under the impetus of concentration gradients by a self-exchange among the occupied and unoccupied electron sites

and thus enhance the electrical conductivity.[40] However, in the next 5 min, all the samples experiences a decrease in the electrical conductivity. This phenomenon has not been observed yet before for conductive polymers. The higher the applied voltage, the faster the electrical conductivity decreases. After removing the voltage, the concentration gradient of electrons introduced by dc potential bias fades gradually, and correspondingly decreases the conductivity. Interestingly, the applied external voltage has no significant effect on the conductivity of metal doped PBZT when the voltage is on, as seen in Figure 5(b). It is suggested that the localization of electrons in polymer is saturated with the donation of electrons by metals and the dc potential bias will not introduce extra electron concentration gradient which would affect the electrical conductivity. However, similar decrease of conductivity is observed after removing the voltage.

3.2 FT-IR

Figure 6 shows the FT-IR spectra recorded in the spectral range of 600-1750 cm^{-1} of PBZT thin films with different doping processes. The peak at 750 cm^{-1} in PBZT is assigned to the N-H wagging vibration in aromatic heterocycle ring.[41] The adjacent peaks at 1540-1650 cm^{-1} represent the unsymmetrical and symmetric bending vibrations of N-H, respectively.[42] This indicates that the nitrogen atom has successfully bound with hydrogen after doping with both acid and metals, i.e. protonation.

The 1484 cm^{-1} band of PBZT corresponds primarily to the C=N stretching vibration.[43] After doping processes, this peak diminishes to a certain degree and suggests a molecular bond transformation from C=N to C-N during the doping process.[30] The decrease of the peak at 1313 cm^{-1} further demonstrates this transformation, which is strongly associated with the reduced polarity after the structure transformation.

3.3 SEM and EDAX analysis

Figure 7(a-e) shows the EDAX elemental analysis of pristine PBZT and PBZT with different doping processes. The silicon element observed in each spectrum is from the silicon substrate. The high peak ration of carbon and sulfur in each spectrum is from PBZT molecules. Obvious chloride (Cl) peak ias observed in all samples, even after doping with different metals, Figure 7(c-e). The elemental analysis of EDAX spectra shows the same elemental peaks for metal doped PBZT and HCl doped PBZT. This indicates that the above observed enhanced electrical conductivity of metal doped PBZT was not caused by metal, but the structural transition of PBZT caused by a reduction process between protonated PBZT and metals. The same color of optical images for different metal doped PBZT also gives some information to explain the same doping mechanism. From the SEM images, the surface of the doped PBZT thin films is smoother and regularly patterned as compared to that of the pristine PBZT. Especially the Pd doped PBZT, no crease is observed on the surface. This indicates a structural transition arising from the doping process.

3.4 XRD

In order to investigate the crystalline structure of the pristine and doped PBZT thin films, XRD measurements are performed. Figure 8(a-e) shows the XRD patterns of the pristine PBZT film and the PBZT films doped with different concentrations of HCl and metals, respectively.

The same peaks at $2\theta = 14.5^{o}$ and 25.5^{o} are observed in the pristine PBZT thin film and the thin film doped with 24.2 wt% HCl, indicating a similar crystalline structure. This indicates that HCl has no significant effect on the crystalline structure of PBZT. The d-spacing is calculated using Bragg's law, Equation (4).[44]

$$d = \frac{n \times \lambda}{2 \sin \theta} \tag{4}$$

where n is chosen as 1, and λ is 1.5406Å for the wavelength of Cu K_α radiation. The calculated d spacing is 6.1 Å and 3.5 Å for 2θ=14.5^o and 25.5^o, respectively. This is consistent with the information from the literature.[23] The peak at 2θ=14.5^o disappears after the PBZT doped with 37 wt% HCl and metals. Meanwhile, two new peaks are observed at 2θ=8.5^o (10.4 Å) and 2θ=17.5^o (5.1 Å), respectively. These indicate a strong influence of high concentration HCl acid and metal doping on the crystalline structures of the PBZT, which is directly observed in the change of surface morphology (Figure 7).

Interestingly, when HCl acid is replaced with H_2SO_4 acid during the same doping process, the similar peak change is observed after doping with 55 wt% H_2SO_4. However, the peak at 2θ=14.5^o appears again after doped with metals while maintaining the two new peaks at 2θ=8.5^o (10.4 Å) and 2θ=17.5^o (5.1 Å), Figure 9. This suggests that the original structure is partially recovered after doping with metals.

3.5 Proposed Structural Change Arising from Doping Process

A molecular structure transformation during doping process is proposed, Figure 10. The nitrogen atom is positively charged through protonation by acid and new carbon-carbon double bond is formed during the reduction process by doping with metal. This transformation shortens the distance between the benzene ring and aromatic heterocycle, and meanwhile doping process decreases the high packing density of the rigid-rod structure. Therefore, both increase at 2θ (17.5^o) and decrease at 2θ (8.5^o) are observed relative to the original 2θ (14.5^o). The XRD patterns for the metal doped samples are in good agreement with the EDAX results, no metal peaks are observed, Figure 7.

4. Conclusion

PBZT films after doping with HCl and H_2SO_4 show switchable conductivity under different sweeping voltages. Generally, the higher concentration of acid, the more efficient switching behavior is observed. After doping with 24.2 wt% HCl, the conductivity of PBZT film is 10 times higher under the sweeping voltage of 0.2~0.3 V than that it is swept at 0~0.1 V. HCl is observed more favorable for a faster and more efficient switching action. Reduction of PBZT with metal (Fe, Cu and Pd) produces a linear conductivity along the whole sweeping range of voltages. Electrons are fully localized on identifiable molecular sites in the polymer and transports under the impetus of concentration gradients by self-exchange between occupied and unoccupied sites, which causes the ohmic electronic conductivity of PBZT.

The external voltage increases the conductivity of acid soaked PBZT by 30% within seconds, and the conductivity maintains stable at the high plateau while keeping on the voltage in the initial 10 min. After removing the voltage, conductivity decreases gradually. Although the conductivity of metal doped PBZT shows voltage-independent even under high external voltage of 10 V, similar degradation is also observed while removing the voltage.

The FT-IR of the formation of N-H peaks and reduction of C=N peak, as well as EDAX elemental analysis and XRD structural analysis indicate that PBZT experiences a structural transition during the protonation and reduction process of PBZT doped with acids and metals.

Acknowledgement

This work was supported by the research start-up fund from Lamar University. The authors appreciate Dr. Y. Mou from Chemistry Department and Dr. J. Gomes from Material Research Center at Lamar University for the FT-IR analysis and for XRD analysis, respectively.

References

1 A. J. Heeger, *J. Phys. Chem. B*, 2001, **105**, 8475-8491.

2 J. L. Bredas and G. B. Street, *Acc. Chem. Res.*, 1985, **18**, 309-315.

3 R. D. McCullough, *Adv. Mater.*, 1998, **10**, 93-116.

4 L. Groenendaal, F. Jonas, D. Freitag, H. Pielartzik and J. R. Reynolds, *Adv. Mater.*, 2000, **12**, 481-494.

5 M. Y. Lebedev, M. V. Lauritzen, A. E. Curzon and S. Holdcroft, *Chem. Mater.*, 1998, **10**, 156-163.

6 M.-Y. Hua, S.-W. Yang and S.-A. Chen, *Chem. Mater.*, 1997, **9**, 2750-2754.

7 A. E. Job, J. A. Giacometti, J. Paulo. S. P. Herrmann and L. H. C. Mattoso, *J. Appl. Phys.*, 2000, **87**, 3878-3882.

8 Y. Berdichevsky and Y.-H. Lo, *Adv. Mater.*, 2006, **18**, 122-125.

9 J. Huang, S. Virji, B. H. Weiller and R. B. Kaner, *Chem. Eur. J.*, 2004, **10**, 1314-1319.

10 J. C. W. Chien and J. B. Schlenoff, *Nature*, 1984, **311**, 362-363.

11 J. C. Carlberg and O. Inganas, *J. Electrochem. Soc.*, 1997, **144**, L61-L64.

12 C. Arbizzani, M. Mastragostino and L. Meneghello, *Electrochim. Acta*, 1996, **41**, 21-26.

13 A. Kros, R. J. M. Nolte and N. A. J. M. Sommerdijk, *Adv. Mater*, 2002, **14**, 1779-1782.

14 B. Rajesh, K. R. Thampi, J.-M. Bonard, H. J. Mathieu, N. Xanthopoulos and B. Viswanathan, *Chem. Commun.*, 2003, 2022-2023.

15 H. Sirringhaus, N. Tessler and R. H. Friend, *Science*, 1998, **280**, 1741-1744

16 S. Gunes, H. Neugebauer and N. S. Sariciftci, *Chem. Rev.*, 2007, **107**, 1324-1338.

17 E. W. Choe and S. N. Kim, *Macromolecules*, 2002, **14**, 920-924.

18 J. F. Wolfe and F. E. Arnold, *Macromolecules*, 2002, **14**, 909-915.

19 J. F. Wolfe, B. H. Loo and F. E. Arnold, *Macromolecules*, 2002, **14**, 915-920.

20 S. R. Allen, A. G. Filippov, R. J. Farris, E. L. Thomas, C. P. Wong, G. C. Berry and E. C. Chenevey, *Macromolecules*, 2002, **14**,1135-1138.

21 R. A. Vaia, J. W. Lee, C. S. Wang, B. Click and G. Price, *Chem. Mater.*, 1998, **10**, 2030-2032.

22 J. A. Osaheni and S. A. Jenekhe, *Macromolecules*, 2002, **27**, 739-742.

23 S.-Y. Park, H. Koerner, S. Putthanarat, R. Ozisik, S. Juhl, B. L. Farmer and R. K. Eby, *Polymer*, 2004, **45**, 49-59.

24 V. V. Kozey, H. Jiang, V. R. Mehta and S. Kumar, *J. Mater. Res.*, 1995, **10**, 1044-1061.

25 D. M. Rein and Y. Cohen, *J. Mater. Sci.*, 1995, **30**, 3587-3590.

26 D. J. Sikkema, *Polymer*, 1998, **39**, 5981-5986.

27 X. Hu, M. B. Polk and S. Kumar, *Macromolecules*, 2000, **33**, 3342-3348.

28 Y.-H. So, B. Bell, J. P. Heeschen, R. A. Nyquist and C. L. Murlick, *J. Polym. Sci., Part A: Polym. Chem.*, 1995, **33**, 159-164.

29 X. Hu, S. Kumar, M. B. Polk and D. L. Vanderhart, *J. Polym. Sci., Part A: Polym. Chem.*, 1998, **36**, 1407-1416.

30 M. F. Roberts, S. A. Jenekhe, A. Cameron, M. McMillan and J. Perlstein, *Chem. Mater.*, 2002, **6**, 658-670.

31 S. A. Jenekhe, P. O. Johnson and A. K. Agrawal, *Macromolecules*, 2002, **22**, 3216-3222.

32 S. A. Jenekhe and P. O. Johnson, *Macromolecules*, 2002, **23**, 4419-4429.

33 J. Song, X. Wang, J. Liu, H. Liu, Y. Li and Z. L. Wang, *Nano Lett.*, 2007, **8**, 203-207.

34 K. Wang, N. L. Rangel, S. Kundu, J. C. Sotelo, R. M. Tovar, J. M. Seminario and H. Liang, *J. Am. Chem. Soc.*, 2009, **131**, 10447-10451.

35 M. D. McClain and D. S. Dudis, *Synth. Met.*, 2001, **116**, 199-202.

36 L. B. Valdes, *Proc. of the IRE*, 1954, **42**, 420-427.

37 F. G. de Souza Jr, B. G. Soares and J. C. Pinto, *Eur. Polym. J.*, 2008, **44**, 3908-3914.

38 K. Wilbourn and R. W. Murray, *J. Phys. Chem.*, 2002, **92**, 3642-3648.

39 N. Minoura, *Langmuir*, 1998, **14**, 2145-2147.

40 P. G. Pickup, W. Kutner, C. R. Leidner and R. W. Murray, *J. Am. Chem. Soc.*, 2002, **106**, 1991-1998.

41 B. C. Smith, *CRC Press: Boca Raton, FL*, 1999, ch. 5, pp. 138-140.

42 M. F. Roberts and S. A. Jenekhe, *Chem. Mater.*, 2002, **5**, 1744-1754.

43 D. Y. Shen and S. L. Hsu, *Polymer*, 1982, **23**, 969-973.

44 Rudel R, Z.-F. F. *J. Physiol.*, 1979, **290**, 317-330.

Figures and Captions

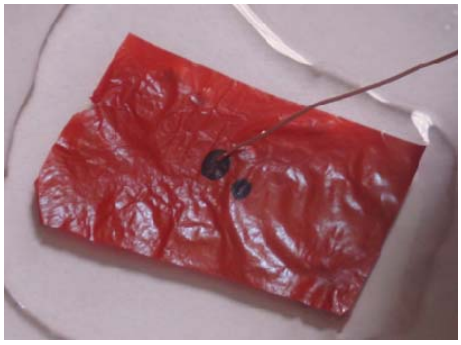

Figure 1 PBZT thin film protonated with 37 wt% HCl and doped with copper.

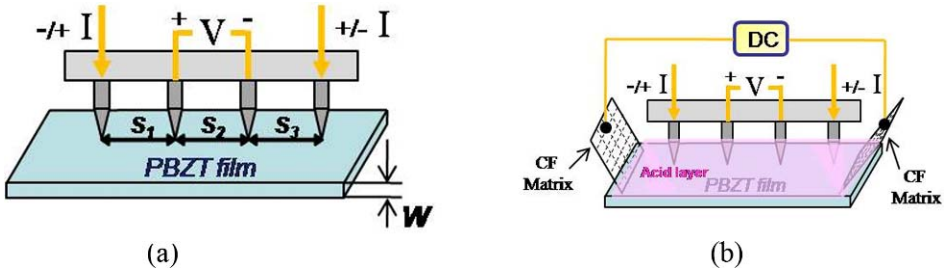

Figure 2 Schematic experimental setup of **(a)** four-probe measurement, and **(b)** four-probe measurement with an applied external voltage.

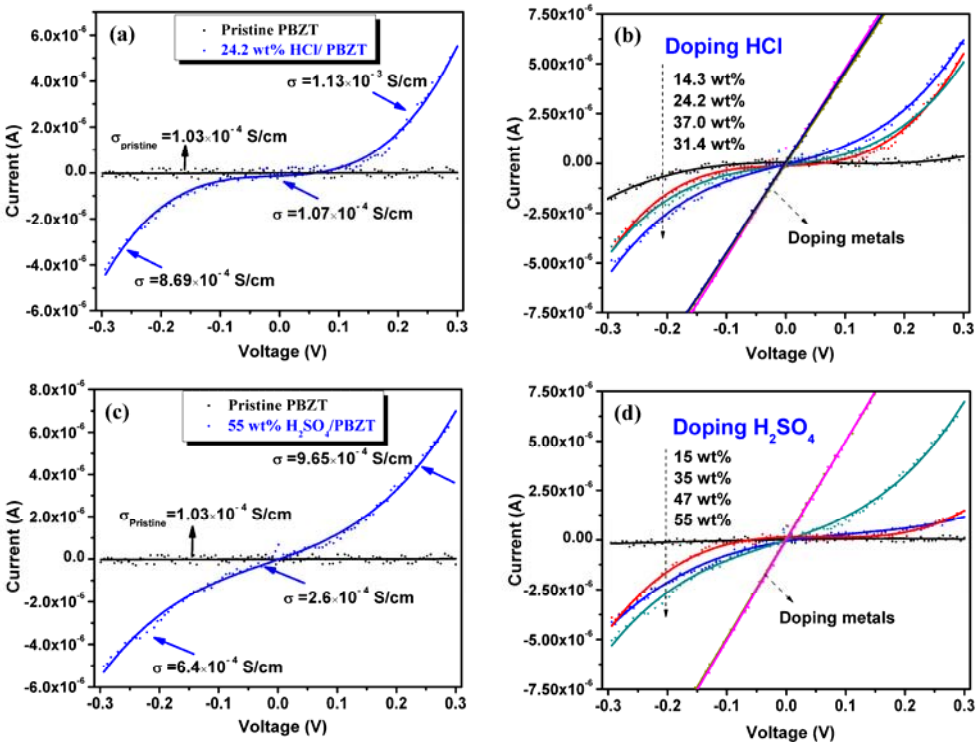

Figure 3 V-I curve of **(a)** 24.2 wt% HCl/PBZT doped and pristine PBZT, **(b)** PBZT doped with different concentrations of HCl and metals, **(c)** 55 wt% H_2SO_4/PBZT doped and pristine PBZT, and **(d**) PBZT doped with different concentrations of H_2SO_4 and metals.

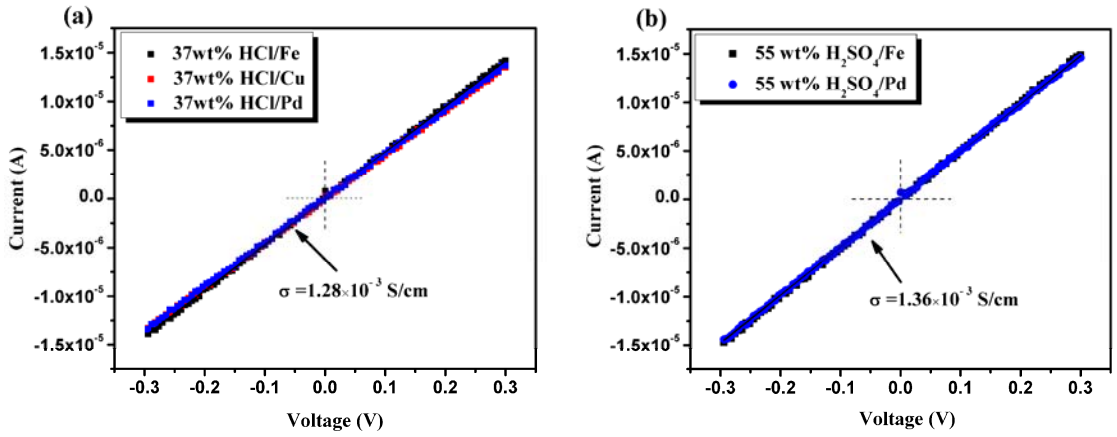

Figure 4 V-I curve of PBZT doped with **(a)** HCl/metal, and **(b)** H_2SO_4/metal

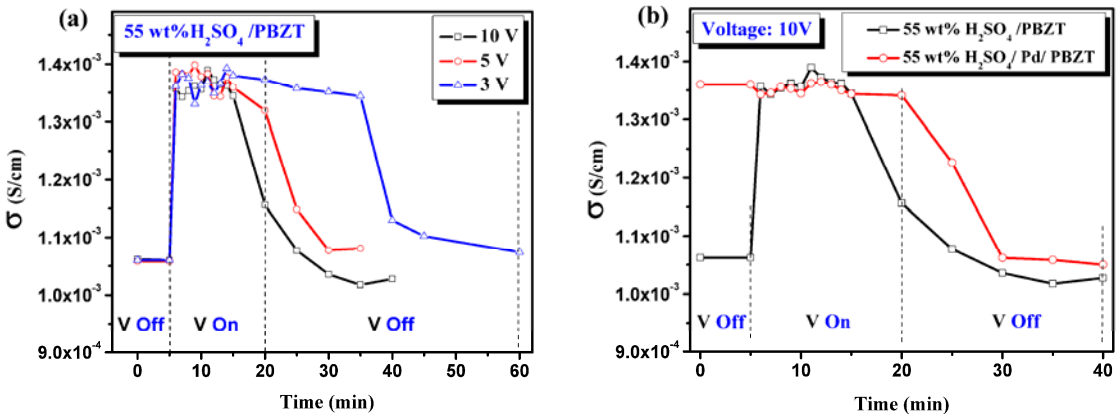

Figure 5 (a) effect of applied external voltages on the electrical conductivity of H_2SO_4 doped PBZT, and **(b)** electrical conductivity for acid, metal doped PBZT films under 10 V external voltage.

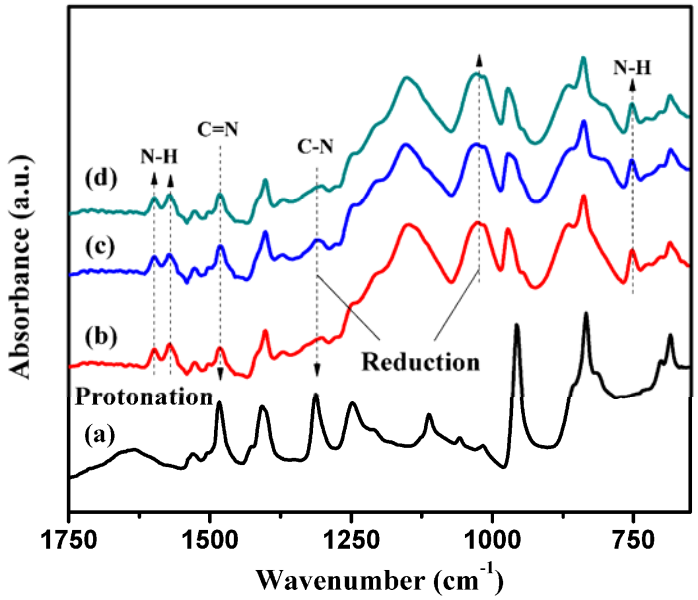

Figure 6 FT-IR spectra of **(a)** pristine PBZT and PBZT thin film doped with **(b)** 55 wt% H_2SO_4, **(c)** 55 wt% H_2SO_4/Fe, and **(d)** 55 wt% H_2SO_4/Pd.

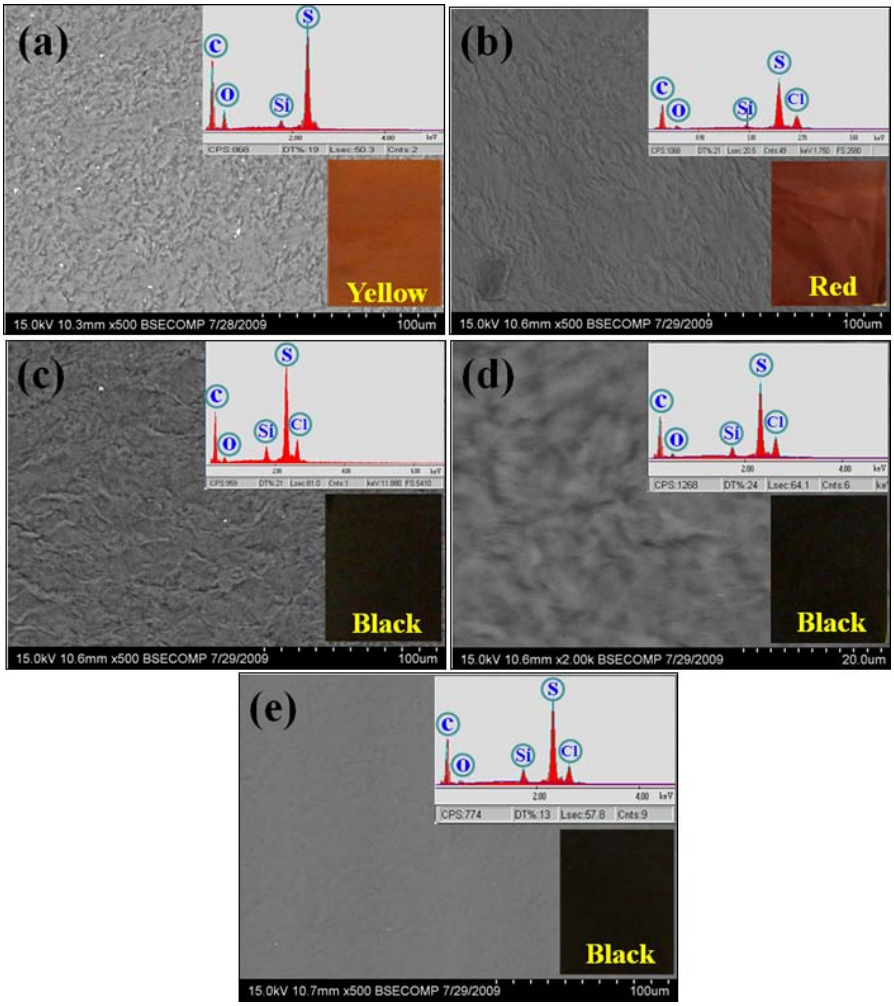

Figure 7 SEM microstructures of **(a)** pristine PBZT, **(b)** 37 wt% HCl/PBZT, **(c)** 37 wt% HCl/Fe/PBZT, **(d)** 37 wt% HCl/Cu/PBZT, and **(e)** 37 wt% HCl/Pd/PBZT. Top inset is the EDAX spectrum obtained from the SEM imaged area. Bottom inset is optical image of PBZT after different doping processes.

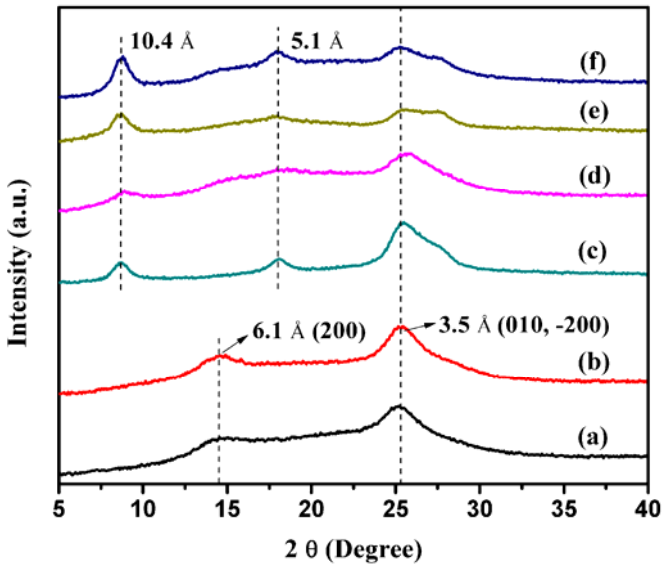

Figure 8 XRD patterns of **(a)** pristine PBZT, and PBZT film doped with **(b)** 24.2 wt% HCl/PBZT, **(c)** 37 wt% HCl/PBZT, **(d)** 37 wt% HCl/Pd/PBZT, **(e)** 37 wt% HCl/Cu/PBZT, and **(f)** 37 wt% HCl/Fe/PBZT.

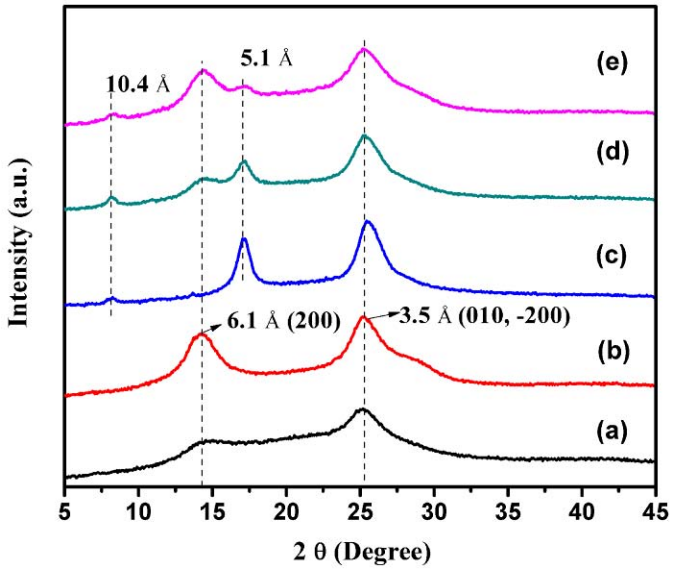

Figure 9 XRD patterns of **(a)** pristine PBZT, and PBZT film doped with **(b)** 15 wt% H_2SO_4/PBZT, **(c)** 55 wt% H_2SO_4/PBZT, **(d)** 55 wt% H_2SO_4/Pd/PBZT, and **(e)** 55 wt% H_2SO_4/Fe/PBZT, respectively.

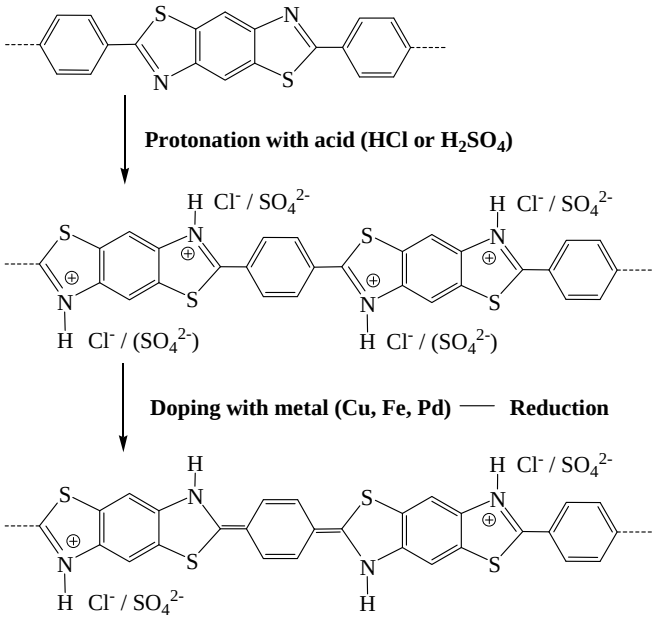

Figure 10 Scheme of protonation and reduction mechanisms of PBZT